Check for updates

A Hybrid Magneto-Optic Capacitive Memory with Picosecond Writing Time

Matthew Rogers, Ahasan Habib, Gilberto Teobaldi, Timothy Moorsom, J. Olof Johansson, Luke Hedley, Paul S. Keatley, Robert J. Hicken, Manuel Valvidares, Pierluigi Gargiani, Nader Alosaimi, Emiliano Poli, Mannan Ali, Gavin Burnell, Bryan J. Hickey, and Oscar Cespedes*

The long-term future of information storage requires the use of sustainable nanomaterials in architectures operating at high frequencies. Interfaces can play a key role in this pursuit via emergent functionalities that break out from conventional operation methods. Here, spin-filtering effects and photocurrents are combined at metal-molecular-oxide junctions in a hybrid magneto-capacitive memory. Light exposure of metal-fullerene-metal oxide devices results in spin-polarized charge trapping and the formation of a magnetic interface. Because the magnetism is generated by a photocurrent, the writing time is determined by exciton formation and splitting, electron hopping, and spin-dependent trapping. Transient absorption spectroscopy measurements show changes in the electronic states as a function of the magnetic history of the device within picoseconds of the optical pumping. The stored information is read using time-resolved scanning magneto optic Kerr effect measurements during microwave irradiation. The emergence of a magnetic interface in the picosecond timescale opens new paths of research to design hybrid magneto-optic structures operating at high frequencies for sensing, computing, and information storage.

1. Introduction

The amount of information stored and circulated doubles approximately every two to four years in what is known as the zettabyte (10^{21} bytes) era.[1] The power required to sustain this evolution in digital information exchange represents a continually increasing percentage of the global resources. In this pursuit, advances have been made to reduce the power required to store and access information whilst increasing the information density and the processing speed. Examples of current developments include spin-orbit transfer torque (SOTT), strain, and capacitive memories.[2] However, these structures face limitations due to the quantum limits in speed and operational power required, e.g. current densities or electrical voltages needed to store and switch information, or the speed of magnetization reversal. Disruptive technologies that can operate at THz frequencies and low power whilst using eco-friendly materials are required to continue this progress in the decades to come. In this drive, the manipulation of spin order using optical irradiation opens research paths towards low-power, high-frequency magnetization storage.[3]

Nanocarbon molecules have been shown to acquire a magnetic moment and modify the behavior of metallic thin films

M. Rogers, A. Habib, T. Moorsom, N. Alosaimi, M. Ali, G. Burnell, B. J. Hickey, O. Cespedes
School of Physics and Astronomy
University of Leeds
Leeds LS2 9JT, UK
E-mail: o.cespedes@leeds.ac.uk

A. Habib
Science, Engineering & Technology School
Khulna University
Khulna 9208, Bangladesh

The ORCID identification number(s) for the author(s) of this article can be found under https://doi.org/10.1002/adfm.202212173.

G. Teobaldi, E. Poli
Scientific Computing Department
Science & Technology Facilities Council UKRI
Rutherford Appleton Laboratory
Didcot OX11 0QX, UK

G. Teobaldi
School of Chemistry
University of Southampton
Southampton SO17 1BJ, UK

J. O. Johansson, L. Hedley
EaStCHEM School of Chemistry
University of Edinburgh
Edinburgh EH9 3FJ, UK

P. S. Keatley, R. J. Hicken
School of Physics
University of Exeter
Exeter EX4 4QL, UK

M. Valvidares, P. Gargiani
ALBA Synchrotron Light Source
E-08290 Barcelona, Spain

via spin-polarized charge transfer and orbital re-hybridization,[4] induce an exchange bias,[5] enhance the spin-orbit coupling,[6] and give raise to emergent spin ordering at the interface with normal metals.[7] The magnetic coupling of molecules with oxides has been on the other hand underexplored, despite the chemical stability and broad range of electronic capabilities of these materials that would make them likely candidates as molecular partners for applications in functional structures. Magnetic metals used as electrodes in hybrid organic semiconducting devices have been shown to give rise to a magnetic-field-dependent photovoltaic effect, adding optical capabilities to molecular spintronics.[8] In fullerene-oxide interfaces an interfacial dipole may be formed due to charge transfer,[9] and this dipole can also lead to exciton splitting and a magnetic-dependent photovoltaic effect.[10] The resultant changes to the spin/electronic structure of the metal and oxide at the molecular interface may give rise to magnetic order, spin filtering, and trapping.[10,11] These emergent functionalities can be used to design information storage and sensing hybrid structures that combine ultra-fast optical processes with low-energy electronics and magnetic stability.

2. Results and Discussion

Here, we present a multi-layered structure where excitons generated by optical excitation in a molecular film are then spin-selective trapped at a metal oxide with non-collinear magnetization. The magnetic information resultant of the spin trapping can be locally generated and stored at molecular-oxide interfaces in the picosecond (ps) scale using optical irradiation. The exciton generated at the molecular layer is split by the dipolar fields at the metal and oxide interfaces. The resultant charge current is spin-selectively blocked from hopping to the oxide, leading to the optical formation of a quasi-2D magnetic layer –**Figure 1**a.

2.1. Photovoltaic Generation of Magnetic Storage

A $Co/C_{60}/MnO_2$ structure generates an open circuit voltage (V_{OC}) of 0.3–0.5 V and short circuit photocurrents (I_{SC}) of 10s mA cm^{-2} when irradiated with ≈10 W cm^{-2} laser light in the visible spectrum (Figure 1b). The fullerene-oxide interface acts
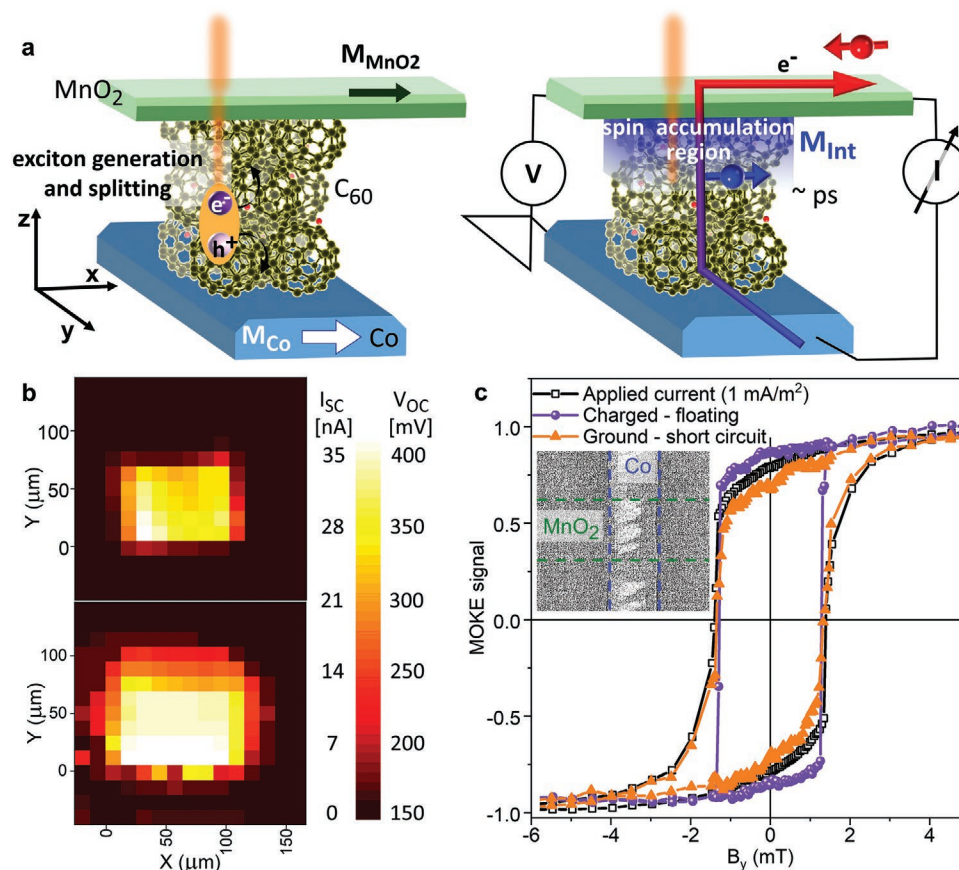

Figure 1. Magneto-optic storage. a) Schematic of the structure. Excitons (pink/purple) are formed in the C_{60} layer during optical irradiation and split due to the dipolar electric fields at the metal- and metal-oxide-molecular interfaces. Electrons may be trapped at the spin-filtering C_{60}/MnO_2 interface. The device can then be charged via light exposure and discharged by grounding the electrodes. b) Photovoltaic characterization of the junction using a 50 µW blue laser (473 nm) focused with a 50x magnification objective. Top: Short-circuit photocurrent I_{sc}. Bottom: Open-circuit voltage V_{OC}. c) MOKE hysteresis loop at the junction region with the magnetic field parallel to the cobalt electrode (magnetization easy axis). When the device is charged, the shape of the loop is changed due to the spin polarized charge trapping and emergent magnetization at the interface. Data before normalization in Figure S9 (Supporting Information). The inset is an optical MOKE image (300 × 300 µm) of the junction region and its magnetic domain structure at the coercive field.

as a spin filter, both layers are calculated to be half-metallic and weakly magnetic. The lack of available states for one spin direction traps electrons when a current flows through the interface. The spin direction of the trapped electrons is determined by coupling to the cobalt electrode. At the cobalt interface, there is also charge transfer and spin-dependent broadening of the molecular levels. When the cobalt electrode is saturated in-plane, the stray field at the interface is well-defined, resulting in efficient filtering and trapping. The trapped polarized charge defines a quasi-2D magnetic interface where information can be stored via electrical or optical irradiation in 1–10 ps. Once the device is shorted, the interface is discharged in timescales of the order of 100 ps and the local magnetization disappears. With the junction in an open circuit, the structure behaves as a magnetic-field-dependent leaky capacitor, with long discharge times of the order of seconds to minutes. The magnetism at the interface can be observed by comparing the remanent magnetization and coercivity of the junction in magneto-optic Kerr effect (MOKE) measurements in the ground and floating,

or charged state –see Figure 1c and Section in the Supporting Information.

2.2. Density Functional Theory and the Effect of Light Polarization

Collinear and non-collinear Density Functional Theory (DFT) simulations of the Co/C_{60}/MnO_2(110) interface were used to unravel the magnetic and electronic properties across the junction. Due to charge transfer and atomic displacements of the oxygen atoms, two electric dipoles (μ) are formed at the molecular interfaces, both pointing toward the oxide electrode –see **Figure 2**a and Supporting Information. These dipoles form the electric field required to break light-generated excitons and give rise to the measured photocurrent, driving electrons from cobalt and the molecular layers toward the manganese oxide. The calculations show that the MnO_2 and its adjacent C_{60} layer (C_{60} 1st) are magnetized, with a half-metallic Density of States
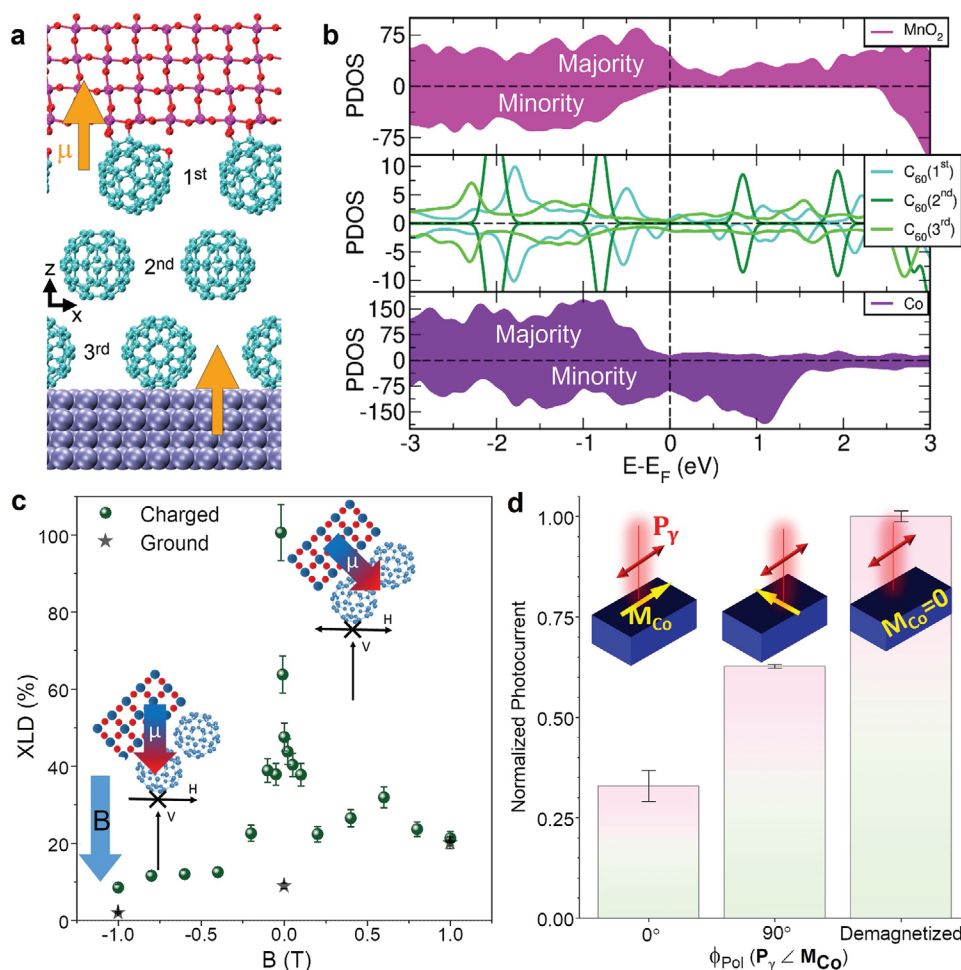
Figure 2. Spin-dependent trapping of photo-generated carriers in Co/C_{60}/MnO_2. a) Modelled structure in DFT calculations, with arrows showing the electric dipoles (μ) formed at the interfaces. b) Collinear DFT atom-projected spin-Polarized Density of States (PDOS) for the Co(0001)/C_{60}/C_{60}/C_{60}/MnO_2(110) interface model. Same C_{60}-labelling as in (a). c) X-Ray absorption spectroscopy linear dichroism at the hybridized carbon K-edge (shifted LUMO due to charge transfer at 282 eV). Once the device is charged, the edge is fully polarized (100% dichroism). The dichroism disappears as a strong magnetic field is applied. d) Short-circuit photocurrent I_{SC} integrated over the device area as a function of the angle θPol between the cobalt magnetization after an applied field (M_{Co}) and the light polarization direction (P_γ).

(DOS), see Figure 2b. The molecular layer on top of the cobalt electrode (C$_{60}$ 3rd) has a small, antiferromagnetic coupling to the metal. Metal and oxide are coupled, with both layers having the same magnetization direction. However, available states for transport near the Fermi level have an opposite spin in the MnO$_2$ and cobalt layers. This leads to trapping and accumulation of the majority of electrons (holes) at the molecular-oxide (-metal) interface when the device is left in a charged/floating state.

X-ray linear dichroism (XLD) measures element-specific differences in the absorption of horizontal and vertical linearly polarized X-rays.[12] Here we used it to probe the orientation of the C$_{60}$ molecular orbitals.[13] We observed a strong XLD signal at the hybridization energy of the C K-edge (≈282 eV) in devices after being charged (Figure 2c; Figure S6, Supporting Information). The dichroism faded when the interfaces was discharged via a common ground, or with an applied magnetic field that can saturate the cobalt electrode 45° out of plane and parallel to the beam. This shows that the geometry of the hybridized molecular orbitals, which control the charge transfer and optical absorption, is coupled to the electric and magnetic state of the junction. With visible light, there is also a dependence of I_{SC} as a function of the angle, θ_{Pol}, between the magnetization of the cobalt electrode, M_{Co}, and the light polarization direction, P_γ. For linearly polarized light and with in-plane magnetization, up to a factor 2 higher I_{SC} was observed for $\theta_{Pol} = 90°$ compared to $\theta_{Pol} = 0°$ (Figure 2d). We attribute this to changes in the effective exciton bandgap as a function of θ_{Pol} due to the

quadratic MOKE effect. Similar effects are observed with circularly polarized light (see Figure S8, Supporting Information). The largest I_{SC} is obtained after degaussing the magnetic electrodes ($M_{Co} = 0$) due to reduced charge trapping and recombination when magnetic disorder is introduced.

2.3. Time Resolved Measurements

We explore the time scales for the formation of the magnetic interface using time-resolved Transient Absorption (TA) spectroscopy[14] as a function of the junction magnetic and electric states.[4c] In this technique, we compare the optical absorption of C$_{60}$ molecules before and after an 80 fs long pump excitation across the HOMO-LUMO gap ($\lambda = 550$ nm). The change in absorbance (ΔA) of C$_{60}$ films after irradiation is probed in the 330–510 nm spectrum and includes a reduced absorbance ($\Delta A < 0$) due to photo bleaching of excitations at 350 nm[15] and electro-absorption generation of charge transfer excitons at 460 and 500 nm.[15,16] An increased absorbance at 400 nm ($\Delta A > 0$) is due to excitations into available estates at the HOMO level and due to absorption from excited electrons (see schematics in **Figure 3**). These features have an initial lower TA response in our devices compared to pristine C$_{60}$ due to the presence of additional layers, photocurrents and charge accumulation. The response time is on the order of sub-ps, which is too fast for thermal effects. Furthermore, the pump-probe signal goes back to zero after each delay scan, meaning that the system has
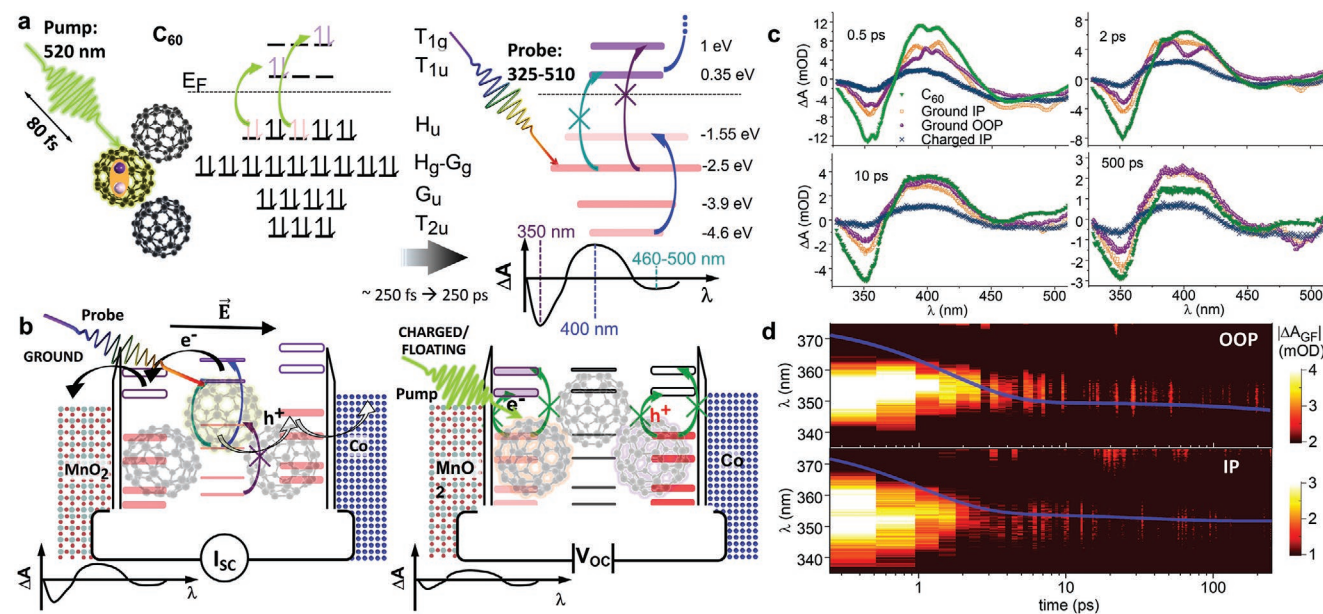
Figure 3. Time-resolved TA spectroscopy in a magneto-photovoltaic structure. Schematic of TA spectroscopy in a pristine C$_{60}$ film a) and in a MnO$_2$/C$_{60}$/Co spin photovoltaic device b) Note that energies are approximate and levels will broaden in proximity to the interfaces.[18] a) Pump irradiation at 520 nm generates excitons by electron promotion from HOMO (Hu) to LUMO (T1u) and LUMO+1 (T1g). The T1u, T1g occupancy reduces the probe absorbance at 350 and 460 nm (HOMO-1 Hg-Gg → T1g, T1u), whereas holes at the HOMO and re-excitation of LUMO states allow for increased absorption at 400 nm. b) In a ground device, changes in absorption (ΔA) are small because carriers are driven to the electrodes by the dipolar electric fields at the interfaces (b-left). In floating devices, the pump cannot excite molecules already charged due to electron accumulation/ trapping at the interface. ΔA is therefore also small, since the probe does not measure strong changes after excitation (b-right). c) TA spectroscopy in the 330–510 nm range measured 0.5 ps, 2 ps, 10 ps, and 500 ps after excitation in a C$_{60}$ film and a Co/C$_{60}$/MnO$_2$ junction in different states. d) Difference in the TA spectrum at 330–380 nm between the charged and the grounded device after an OOP (top) or IP magnetic field (bottom). The blue line insets show $|\Delta A_{GF}|$ fit to a double exponential decay with the main time constants of 1.3 ± 0.2 ps; 40 ± 10 ps (OOP) or 2 ± 0.3 ps; 400 ± 200 ps (IP).

relaxed between each consecutive pump-probe pulse (1 ms). This excludes any long-term thermal effects.

Ground devices give raise to a photocurrent that splits the excitons generated by the pump, so that carriers diffuse toward the electrodes and the molecules can be re-excited by the probe signal. Since new excitons can be created, the changes in absorption from pump to probe (ΔA) are smaller than for pristine C_{60}. As shown in Figure 2, magnetically disordered junctions generated larger photocurrents. The recombination of well-defined spin polarized electrons trapped at the C_{60}-MnO_2 interface with opposite spin holes leads to a lower ΔA signal at 350 nm when the magnetization M was disordered by an out-of-plane (OOP) magnetic field (M ≈ $0.2M_S$, with M_S the saturation magnetisation) than when the junction was magnetised in-plane (IP; M ≈ M_S). ΔA was yet smaller in floating devices, where interface molecules are excited before the pump irradiation due to charge trapping and accumulation. These changes can be observed in sub-ps timescales, and in our devices persist for the duration of the measurement. For pristine C_{60} films, after several 100 ps exciton recombination leads to a sharp drop in ΔA, Figure 3c, Figures S10 and S14 (Supporting Information).

The time to accumulate charge and form the magnetic interface was estimated comparing the absorption change between ground (charge/discharge) and floating (charged steady state) junctions: $|\Delta A_{GF}| \equiv |\Delta A_{Ground} - \Delta A_{Floating}|$. With an OOP magnetically disordered junction, $|\Delta A_{GF}|$ drops with a characteristic timescale of 1.3 ± 0.2 ps. In IP magnetically saturated devices with higher recombination and lower photocurrent, $|\Delta A_{GF}|$ has a timescale of 2.0 ± 0.3 ps. The difference is in good agreement with the relative photocurrents for each magnetic configuration –Figure 2d. This timescale would correspond to the electron

hopping from C_{60} to the hybridized interface and the formation of the magnetic interface due to spin accummulation.[15,17] A second, smaller and slower decay of 10s to 100s ps can be attributed to the diffusion of charges across the C_{60} film to the interface and exciton recombination (Figure 3d; Figure S13, Supporting Information).

To probe (read) the local magnetization at the C_{60}-MnO_2 interface, we use Time-Resolved Scanning Kerr Microscopy (TRSKM) –see Ref. [19] The setup can measure the spin pumping during ferromagnetic resonance at the junction. A waveguide generates a short magnetic field pulse, generating an oscillation of the magnetization in cobalt at the resonant frequency corresponding to the applied external field. The damping of this oscillation is correlated with the transfer of angular momentum to the other layers, and is dependent on the charged state of the interface, see **Figure 4**a for a schematic of the experimental setup.

As seen above, the spin-polarized charge accumulated at the interface, and therefore the magnetic information stored, depends on the relative alignment of the light polarization used to generate the photocurrent with respect to the magnetization of the cobalt electrode. For parallel configurations, the amount of charge accumulated is larger (smaller photocurrent), which will lead to a more magnetic interface. TRSKM data in optically irradiated $Co/C_{60}/MnO_2$ junctions can be fitted with two effective magnetizations, one correspondi.ng to the Co layer with a value of ≈865 ± 50 emu cc^{-1} (statistically unchanged by the polarization of the light used) and another with a value of 3000 ± 600 or 4300 ± 100 emu cc^{-1} for θ_{Pol} = 90° or θ_{Pol} = 0°, respectively (Figure 4b). See Section V (Supporting Information) for details on the data analysis. We identify this second
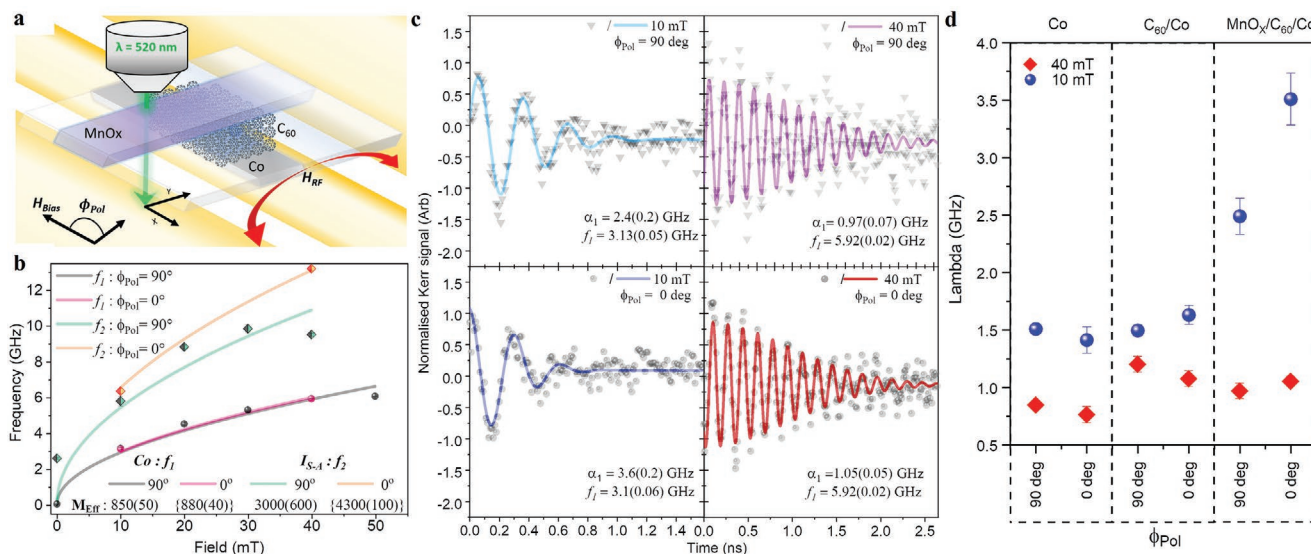
Figure 4. Microwave detection of the photo-generated magnetic interface. a) Schematic of the TRSKM experiment. b) Plot of the ferromagnetic resonance frequency in the $Co/C_{60}/MnO_2$ junction as a function of the applied field where the data is modelled by two independent oscillating magnetic layers. c) Time-resolved magnetization precession at 10 mT (magnetization axis of the charged layer determined by the cobalt electrode stray field) and 40 mT (charged layer aligned with the external field) at 90° and 0°. d) Ferromagnetic resonance damping (lambda), indicative of efficient spin pumping and the formation of a magnetized layer at the C_{60}/MnO_2 interface. Higher damping, and therefore magnetic transfer, is observed at the junction region when exposed to light polarized parallel to M_{Co} in an external field of 10 mT. At a higher field of 40 mT the C_{60}/MnO_2 interface is parallel to the Co electrode and no spin accumulation takes place. Error bars not shown are smaller than the point size. For c,d) the magnetization precession is modelled with a more robust single-frequency model.

**ADVANCED
SCIENCE NEWS**
www.advancedsciencenews.com

**ADVANCED
FUNCTIONAL
MATERIALS**
www.afm-journal.de

magnetization with the charged layer at the interface, which has a higher density of charge trapping when the light is polarized parallel to the cobalt magnetization. The time-resolved magnetization precession at different fields and light polarizations is shown in Figure 4c and 4d.

In a simplified model that assumes a single oscillating magnetization, a change in the precession damping (lambda) as a function of the light polarization, magnetic field and region of the sample is observed (Figure 4c,d; Figures S16 and S17, Supporting Information). Outside the junction, the damping does not depend on light polarization. In the junction, at 40 mT the interface magnetization is aligned with the external field. The damping is then similar to that measured in Co/C_{60} and independent of the light polarization. At 10 mT, the stray field determines the magnetization of the interface and electrons with spin parallel to the cobalt magnetization are trapped. The trapped charge increases when the light polarization is parallel to the cobalt magnetization, which is detected by the enhanced damping (Figure 4d).

3. Conclusion

We have given proof of concept for the formation of a local magnetic interface in C_{60}/MnO_2 grown on a magnetic metal electrode due to spin-polarized charge accumulation when exposed to visible light irradiation. The photocurrent generated is dependent on the relative alignment of the light polarization and the magnetization of the metal, which can be used in magneto-optic and polarization sensors. The charge accumulation takes place in timescales of the order of ps, with the resultant emergent magnetic interface probed via spin pumping at GHz frequencies. The discharge can be in 100s ps or several minutes-hours depending on whether the electrodes are shorted or disconnected, but remain charged indefinitely if disconnected under optical exposure. Our measurements reveal the connections between molecular excitations, charge trapping and the emergence of spin order at sub-ps to ns timescales. The results open new paths of research for the design and implementation of eco-friendly, ultra-fast hybrid memories operated via light or electrical irradiation at THz frequencies.

4. Experimental Section

All layers of the device were grown in situ without breaking vacuum at a base pressure of $\approx 10^{-8}$ mTorr. Electrodes were deposited via DC magnetron sputtering (Co) and plasma oxidation (MnO_2) on a transparent insulating substrate. C_{60} had a long spin coherence time and was highly resilient to the sputtering on top of metals and plasma oxidation. It had a low vapour pressure compatible with UHV growth, and layers were deposited in situ via thermal evaporation at ≈ 450 °C. The films were polycrystalline, with a grain size of several 10s of nm. Devices had a resistance of $\approx M\Omega$ at low voltages for a typical 100×100 μm^2 junction area. The high resistance reduces the photocurrent but improves the information storage effect via the spin polarized trapped electrons. A thermal voltage and current can be measured upon laser excitation, but these are orders of magnitude smaller than the photovoltaic effect. Unlike the current and voltage generated by photoexcited carriers, the polarity of the thermal voltage/current is dependent on whether the light is incident on the oxide or the metal (front or back of sample) and can therefore be trivially excluded. XAS and XMCD

spectra(data) were measured in the BOREAS beamline at the ALBA synchrotron.[20] The X-ray beam was produced by an elliptically polarized undulator and monochromatized by a variable line spacing grating monochromator (400 lines mm^{-1} at Carbon edge), with a total flux of the order of 10^{11} photons s^{-1} at the Carbon edge. The beam was collimated by variable focusing bender mirrors down to $\approx 100 \times 50$ microns, allowing the junction area to be accurately located via triangulation with the electrodes, further detail can be found in the Supporting Information.

The details of the transient absorption spectrometer have been reported elsewhere.[16] Briefly, the 120 fs 800 nm output from a Coherent Legend Elite, operating at 1 kHz, was directed into a non-collinear optical parametric amplifier to produce 550 nm 80 fs pump pulses. The pulse fluence at the sample was 1.8 mJ cm^{-2}. A small portion of the 800 nm output was focused into a CaF_2 plate to generate a white-light continuum, which was further split into a probe and reference beam. Each of these beams were sent to two home-built prism spectrometers equipped with CCD cameras (Entwicklungsbuero Stresing) operating at 1 kHz.

Time-resolved polar Kerr measurements in response to a pulsed magnetic field were performed at normal incidence in a scanning microscope. Probing laser pulses were generated from a mode-locked fiber laser with a repetition rate of 80 MHz and pulse duration of 140 fs at a wavelength of 1040 nm. Magnetization dynamics were probed at the second harmonic wavelength of 520 nm attenuated to an average power of not >1 mW before the microscope objective lens. Probe pulses were linearly polarized and focused to a microscale spot using either a x10 objective lens or a 40 mm plano-convex lens. The time delay of the probing laser pulses with respect to the pulsed magnetic field excitation was set using an 8 ns optical delay line with sub-ps resolution. The 80 MHz laser sync output was used as a clock input for an impulse generator to generate electrical pulses with ≈ 5 V amplitude, and 70 ps duration that were synchronous with the probe laser pulses. The electrical pulses were passed through a coplanar waveguide with center conductor width of either 0.5 or 1 mm. The associated in-plane pulsed magnetic field above the center conductor was then used to excite magnetization dynamics in the device that was placed face down upon the waveguide, while the in-plane equilibrium magnetic state of the device was set using either a tri-pole 3D projected field electromagnet, or a stack of permanent magnets mounted on a translation stage. The polar magneto-optical Kerr effect was then used to probe the dynamic state of the out-of-plane component of the magnetization as a function of optical time delay in time-resolved Kerr measurements. The Kerr measurements were probed through a transparent substrate so that the device was in good proximity with the coplanar waveguide and excitation field. Polar Kerr signals corresponding to the change in the out-of-plane component of the dynamic magnetization were detected using a balanced photodiode polarizing bridge detector with a 1 MHz bandwidth. Modulation of the pulsed field excitation at ≈ 30 kHz allowed the modulated change in the polar Kerr rotation to be recovered using a lock-in amplifier with ≈ 10 μdeg resolution.

Supporting Information

Supporting Information is available from the Wiley Online Library or from the author.

Acknowledgements

Conflict of Interest

The authors declare no conflict of interest.

Data Availability Statement

The data that support the findings of this study are openly available in Research Data Leeds Repository at https://doi.org/10.5518/1256, reference number 852.

Keywords

information storage, molecular spintronics, photovoltaics, THz devices

[1] a) G. S. Kar, A. Furnemont, *Solid State Technol.* **2018**, *61*, 14; b) A. M. Ionescu, presented at *63rd IEEE Annual Int. Electron Devices Meeting (IEDM)*, San Francisco, CA, Dec 02–06 **2017**.

[2] P. Nemec, E. Rozkotova, N. Tesarova, F. Trojanek, E. De Ranieri, K. Olejnik, J. Zemen, V. Novak, M. Cukr, P. Maly, T. Jungwirth, *Nat. Phys.* **2012**, *8*, 411.

[3] a) B. Nafradi, P. Szirmai, M. Spina, H. Lee, O. V. Yazyev, A. Arakcheeva, D. Chernyshov, M. Gibert, L. Forro, E. Horvath, *Nat. Commun.* **2016**, *7*, 13406; b) Y. F. Zhao, S. S. Zhao, L. Wang, Z. Y. Zhou, J. X. Liu, T. Min, B. Peng, Z. Q. Hu, S. Y. Jin, M. Liu, *Adv. Sci.* **2019**, *6*, 1901994; c) B. Nafradi, P. Szirmai, M. Spina, A. Pisoni, X. Mettan, N. M. Nemes, L. Forro, E. Horvath, *Proc. Natl. Acad. Sci. USA* **2020**, *117*, 6417.

[4] a) O. Cespedes, M. S. Ferreira, S. Sanvito, M. Kociak, J. M. D. Coey, *J. Phys.: Condens. Matter* **2004**, *16*, L155; b) T. L. A. Tran, P. K. J. Wong, M. P. de Jong, W. G. van der Wiel, Y. Q. Zhan, M. Fahlman, *Appl. Phys. Lett.* **2011**, *98*, 222505; c) T. Moorsom, M. Wheeler, M. T. Khan, F. Al Ma'Mari, G. Burnell, B. J. Hickey, V. Lazarov, D. Gilks, O. Cespedes, *Appl. Phys. Lett.* **2014**, *105*, 022408.

[5] M. Gruber, F. Ibrahim, S. Boukari, H. Isshiki, L. Joly, M. Peter, M. Studniarek, V. Da Costa, H. Jabbar, V. Davesne, U. Halisdemir, J. J. Chen, J. Arabski, E. Otero, F. Choueikani, K. Chen, P. Ohresser, W. Wulfhekel, F. Scheurer, W. Weber, M. Alouani, E. Beaurepaire, M. Bowen, *Nat. Mater.* **2015**, *14*, 981.

[6] S. Alotibi, B. J. Hickey, G. Teobaldi, M. Ali, J. Barker, E. Poli, D. D. O'Regan, Q. Ramasse, G. Burnell, J. Patchett, C. Ciccarelli, M. Alyami, T. Moorsom, O. Cespedes, *Acs Appl. Mater. Interfaces* **2021**, *13*, 5228.

[7] a) F. Al Ma'Mari, T. Moorsom, G. Teobaldi, W. Deacon, T. Prokscha, H. Luetkens, S. Lee, G. E. Sterbinsky, D. A. Arena, D. A. MacLaren, M. Flokstra, M. Ali, M. C. Wheeler, G. Burnell, B. J. Hickey, O. Cespedes, *Nature* **2015**, *524*, 69; b) F. Al Ma'Mari, M. Rogers, S. Alghamdi, T. Moorsom, S. Lee, T. Prokscha, H. Luetkens, M. Valvidares, G. Teobaldi, M. Flokstra, R. Stewart, P. Gargiani, M. Ali, G. Burnell, B. J. Hickey, O. Cespedes, *Proc. Natl. Acad. Sci. USA* **2017**, *114*, 5583; c) F. Djeghloul, M. Gruber, E. Urbain, D. Xenioti, L. Joly, S. Boukari, J. Arabski, H. Bulou, F. Scheurer, F. Bertran, P. Le Fevre, A. Taleb-Ibrahimi, W. Wulfhekel, G. Garreau, S. Hajjar-Garreau, P. Wetzel, M. Alouani, E. Beaurepaire, M. Bowen, W. Weber, *J. Phys. Chem. Lett.* **2016**, *7*, 2310.

[8] a) X. N. Sun, S. Velez, A. Atxabal, A. Bedoya-Pinto, S. Parui, X. W. Zhu, R. Llopis, F. Casanova, L. E. Hueso, *Science* **2017**, *357*, 677; b) K. Bairagi, D. G. Romero, F. Calavalle, S. Catalano, E. Zuccatti, R. Llopis, F. Casanova, L. E. Hueso, *Adv. Mater.* **2020**, *32*, 1906908.

[9] J. P. Prieto-Ruiz, S. G. Miralles, N. Grossmann, M. Aeschlimann, M. Cinchetti, H. Prima-Garcia, E. Coronado, *Adv. Electron. Mater.* **2017**, *3*, 1600366.

[10] T. Moorsom, M. Rogers, I. Scivetti, S. Bandaru, G. Teobaldi, M. Valvidares, M. Flokstra, S. Lee, R. Stewart, T. Prokscha, P. Gargiani, N. Alosaimi, G. Stefanou, M. Ali, F. Al Ma'Mari, G. Burnell, B. J. Hickey, O. Cespedes, *Sci. Adv.* **2020**, *6*, eaax1085.

[11] a) M. C. Wheeler, F. Al Ma'Mari, M. Rogers, F. J. Goncalves, T. Moorsom, A. Brataas, R. Stamps, M. Ali, G. Burnell, B. J. Hickey, O. Cespedes, *Nat. Commun.* **2017**, *8*, 926; b) K. V. Raman, A. M. Kamerbeek, A. Mukherjee, N. Atodiresei, T. K. Sen, P. Lazic, V. Caciuc, R. Michel, D. Stalke, S. K. Mandal, S. Blugel, M. Munzenberg, J. S. Moodera, *Nature* **2013**, *493*, 509; c) S. Javaid, M. Bowen, S. Boukari, L. Joly, J. B. Beaufrand, X. Chen, Y. J. Dappe, F. Scheurer, J. P. Kappler, J. Arabski, W. Wulfhekel, M. Alouani, E. Beaurepaire, *Phys. Rev. Lett.* **2010**, *105*, 077201; d) F. Ngassam, E. Urbain, L. Joly, S. Boukari, J. Arabski, F. Bertran, P. Le Fevre, G. Garreau, P. Wetzel, M. Alouani, M. Bowen, W. Weber, *J. Phys. Chem. C* **2019**, *123*, 26475.

[12] a) G. Vanderlaan, B. T. Thole, G. A. Sawatzky, J. B. Goedkoop, J. C. Fuggle, J. M. Esteva, R. Karnatak, J. P. Remeika, H. A. Dabkowska, *Phys. Rev. B* **1986**, *34*, 6529; b) J. Stöhr, *Springer Ser. Surf. Sci.* **1992**, *25*, 276.

[13] J. Stohr, H. A. Padmore, S. Anders, T. Stammler, M. R. Scheinfein, *Surf. Rev. Lett.* **1998**, *5*, 1297.

[14] a) F. Liedy, J. Eng, R. McNab, R. Inglis, T. J. Penfold, E. K. Brechin, J. O. Johansson, *Nat. Chem.* **2020**, *12*, 452; b) P. Foggi, L. Bussotti, F. V. R. Neuwahl, *Int. J. Photoenergy* **2001**, *3*, 103.

[15] M. Causa, I. Ramirez, J. F. M. Hardigree, M. Riede, N. Banerji, *J. Phys. Chem. Lett.* **2018**, *9*, 1885.

[16] a) S. V. Chekalin, A. P. Yartsev, V. Sundstrom, *Quantum Electron.Electron.* **2001**, *31*, 395; b) T. E. Saraswati, U. H. Setiawan, M. R. Ihsan, I. Isnaeni, Y. Herbani, *Open Chem.* **2019**, *17*, 1198.

[17] S. Emmerich, S. Hedwig, B. Arnoldi, J. Stockl, F. Haag, R. Hemm, M. Cinchetti, S. Mathias, B. Stadtmuller, M. Aeschlimann, *J. Phys. Chem. C* **2020**, *124*, 23579.

[18] a) S. Sanvito, *Nat. Phys.* **2010**, *6*, 562; b) C. Barraud, P. Seneor, R. Mattana, S. Fusil, K. Bouzehouane, C. Deranlot, P. Graziosi, L. Hueso, I. Bergenti, V. Dediu, F. Petroff, A. Fert, *Nat. Phys.* **2010**, *6*, 615.

[19] P. S. Keatley, V. V. Kruglyak, P. Gangmei, R. J. Hicken, *Philos. Trans. R. Soc., A* **2011**, *369*, 3115.

[20] A. Barla, J. Nicolas, D. Cocco, S. M. Valvidares, J. Herrero-Martin, P. Gargiani, J. Moldes, C. Ruget, E. Pellegrin, S. Ferrer, *J. Synchrotron Radiat.* **2016**, *23*, 1507.